Research Article Vol. 3, No. 2 / 15 Feb 2024 / Optics Continuum 112

OPTICS CONTINUUM

Beam quality improvement in a linear ZPG OPO pumped by a Q-switched compact high-power Ho^{3+}:YAG laser

KATHARINA GOTH,[1,2,*] MADELEINE EITNER,[2] MICHAEL GRIESBECK,[2] MARIUS RUPP,[1,2] DOMINIK LORENZ,[1,2] JOHANNES DEUTSCH,[1,2] MARC EICHHORN,[1,2] AND CHRISTELLE KIELECK[1,2]

[1]*Fraunhofer IOSB (Institute of Optronics, System Technologies and Image Exploitation), Gutleuthausstraße 1, 76275 Ettlingen, Germany*

[2]*Institute of Control Systems, Karlsruhe Institute of Technology, Fritz-Haber-Weg 1, 76131 Karlsruhe, Germany*

[*]*katharina.goth@iosb-extern.fraunhofer.de*

Abstract: We present a Ho^{3+}:YAG laser pumped by a Tm^{3+}-doped fiber laser that delivers pulses with an energy of 2.2 mJ and a pulse duration of 20 ns at a repetition rate of 25 kHz. The average output power is 58 W, while the pulse peak power is 108 kW. This source is used to pump a linear zinc germanium phosphide optical parametric oscillator (OPO) in different configurations. The resonators are investigated with a focus on maximum output power and beam quality. By introducing a diverging lens in the OPO cavity, the beam quality of signal and idler is improved significantly. For a pump power of 34 W, a combined mid-infrared output power of 14.1 W corresponding to a pulse energy of 0.56 mJ is obtained. For this output power, beam quality factors M^2 in the x- and y-axis of 2.1 and 3.3 as well as 2.4 and 3.5 are achieved for the signal and idler beam, respectively.

1. Introduction

High-power coherent light sources in the 3 - 5 µm mid-infrared (mid-IR) region are required for applications like remote sensing, medical diagnostics [1], material processing [2], or optical countermeasures [3]. Different laser sources directly emit in the mid-IR wavelength range, for example quantum-cascade lasers based on InGaAs [4] as well as Er^{3+}:ZrF_4 or Ho^{3+}:InF_3 fiber lasers [5,6]. Nevertheless, these direct emitters lack power scalability and especially the capability to generate high-energy nanosecond pulses. The same holds true for Fe^{2+}:ZnSe lasers emitting around 4 – 5µm [7,8] as well as Dysprosium-doped solid-state lasers [9]. Another possibility to access the mid-IR range is the nonlinear conversion of 2 µm light in optical parametric oscillators (OPOs), an approach already proven to significantly scale the mid-IR output in both average power and pulse energy [10,11]. As a consequence of energy conservation, while only the signal band of the OPO is found in the near-infrared wavelength range in the case when a laser source emitting around 1 µm is used, both OPO output bands are located in the mid-IR region when the pump source is a 2 µm laser. These laser sources can be used to pump zinc germanium phosphide (ZGP) crystals that require pump sources with a wavelength above 2 µm, limited due to the strong absorption below 2 µm [12]. ZGP has outstanding properties to serve as a nonlinear crystal in OPOs since it has a high nonlinear coefficient (d_{36} = 75 pm/V) and a high thermal conductivity [13,14].

Suitable pump sources for ZGP OPOs are ns-pulsed holmium-doped yttrium-aluminum-garnet (Ho^{3+}:YAG) crystal lasers emitting around 2.1 µm due to a variety of reasons: besides a highly efficient pumping scheme involving Tm^{3+}-doped fiber lasers emitting at 1908 nm, the long upper-state lifetime of the Ho^{3+}-ion [15] enables an efficient energy extraction in Q-switched

#505473 https://doi.org/10.1364/OPTCON.505473
Journal © 2024 Received 11 Sep 2023; revised 9 Dec 2023; accepted 11 Dec 2023; published 18 Jan 2024

OPTICS CONTINUUM

operation and therefore, high pulse energies can be generated [16]. Furthermore, with an optimized cavity design, an excellent beam quality can be achieved in these lasers [17] which is a requirement for developing OPOs with high conversion efficiencies.

ZGP OPOs pumped by Ho^{3+}-doped crystal lasers have been subject to research in the last decades. OPO architectures ranging from simple linear resonators over ring resonators to fractional-image-rotation enhancement resonators have been presented [10,18–20]. While linear resonators are characterized by their low complexity and compactness, the required use of optical isolators to protect the pump laser from back reflections limits the available pump power. 12.6 W of output power have been shown in a linear ZPG OPO with one nonlinear crystal [21]. In a linear ZGP OPO with two walk-off compensated crystals, 24.2 W of OPO output power have been generated with a beam quality of $M^2 = 3.1$ measured at 20 W of OPO output power [22]. An optical isolator is not required in ring resonators, which enables higher pump and output powers, but on the other hand ring resonators have a higher complexity. Up to 78 W of output power with a beam quality of $M^2 \approx 3$ have been shown in a ZGP OPO pumped by a Ho^{3+}:YAG master oscillator power amplifier system [10]. As can be seen from the beam quality factors mentioned, maintaining a good beam quality even at elevated pulse energies and output powers remains a challenging task both in linear resonators as well as in ring resonators. The reason for this lies in the mismatch between the small resonator mode diameters in the typically short OPO cavities influenced by thermal lensing and gain guiding in the ZGP crystal [23] and the large pump diameters required at high pump powers to remain below the damage threshold of the components. An appropriate measure to address this issue is the use of an intracavity lens as has been shown in a ZGP ring resonator by Qian et al. in 2019 [24]. However, to the best of our knowledge, this has not yet been shown for a linear ZGP OPO.

In this paper, we investigate this topic, starting with the presentation of the setup of our Ho^{3+}:YAG source in Sec. 2, followed by its characterization in Sec. 3. The experimental setup of the ZGP OPO is shown in Sec. 4, while the investigation of the different resonator configurations is presented in Sec. 5. The paper concludes with a discussion and a summary of the most significant findings in Sec. 6.

2. Experimental setup of Ho^{3+}:YAG pump source

The Ho^{3+}:YAG laser source is shown in Fig. 1. A commercially available 100 W Tm^{3+}-doped fiber laser emitting at 1908 nm with a beam quality of M^2<1.1 pumps the $^5I_8 \rightarrow {}^5I_7$ transition of the Ho^{3+}:YAG crystal. A thorough investigation of this resonator already been presented in [25]. The pump beam is focused into the Ho^{3+}:YAG crystal with a $1/e^2$ pump beam diameter around 500 - 600 µm by a Gaussian telescope, which consists of the lenses L_1 and L_2, to enable mode matched operation. It is coupled into the resonator using a dichroic input coupling mirror (IC) which is highly reflective (HR) (R>99.9 %) at the pump wavelength and has R<2 % for the p-polarization of the 2090 nm light. It is also highly reflective (R>99%) for the s-polarization

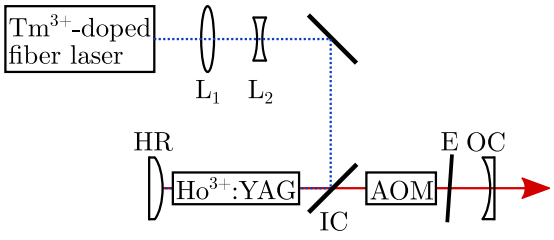

Fig. 1. Schematic representation of the Ho^{3+}:YAG laser setup. Abbreviations are explained in the text.

OPTICS CONTINUUM

of the 2090 nm light which introduces high losses at this polarization and ensures the linear polarization of the Ho^{3+}:YAG laser. The 28 mm long Ho^{3+}:YAG crystal with an undoped end cap is mounted in a copper mount which is water-cooled to 20 °. The doping concentration of the crystal was optimized for an efficient pump light absorption. The cavity is built by a convex HR mirror with a radius of curvature of −0.25m and a concave output coupling (OC) mirror with a radius of curvature of 0.3m and a reflectivity of 50%. The HR mirror has a high reflectivity for both the pump and the laser light resulting in a double-pass of the pump light through the crystal which improves the pump light absorption and, therefore, the efficiency of the system. The total physical length of the cavity is 9.8 cm. Q-switched operation is enabled by a TeO_2 acousto-optic modulator (AOM) mounted inside the resonator between the IC mirror and the OC mirror. Next to it, an 80 µm thick fused silica etalon ensures an efficient operation of the laser at the 2090 nm spectral line. The following section presents a characterization of this laser source in both continuous-wave and Q-switched operation.

3. Characterization of Ho^{3+}:YAG pump source

Figure 2(a) shows the output power of the Ho^{3+}:YAG pump source in continuous-wave operation. It has a high slope efficiency of 67.6 % and low pump threshold of 3.7 W. A maximum output power of 62 W is reached at a pump power of 99 W. The working point of the Ho^{3+}:YAG laser is set to a pump power of 89 W yielding an output power of 58 W since a good mode matching between pump and laser mode is established. At this working point, an excellent beam quality of M^2<1.1 results in both the x- and y-axis of the beam. This also holds true for the operation in the quasi-continuous regime at a pulse repetition rate of 50 kHz (see Fig. 2(b)). The beam quality was measured by focusing the laser beam with a plano-convex lens and measuring the $1/e^2$ beam diameter at different positions of the resulting beam caustic. The astigmatism of the beam most likely results from the thermally induced birefringence in the crystal and the laser beam passing through the IC mirror at an oblique angle. Since the crystal rod has a cylindrical shape, the thermally induced stress builds up in a radial and tangential eigensystem. Due to the linear polarization of the laser mode, the thermally induced birefringence leads to a bifocusing of the thermal lens which explains the first contribution to the astigmatism [26]. The second contribution results from the axial asymmetry due to the tilted mirror inside the laser cavity which effectively results in different resonator lengths for the two beam axes [27]. This effect is

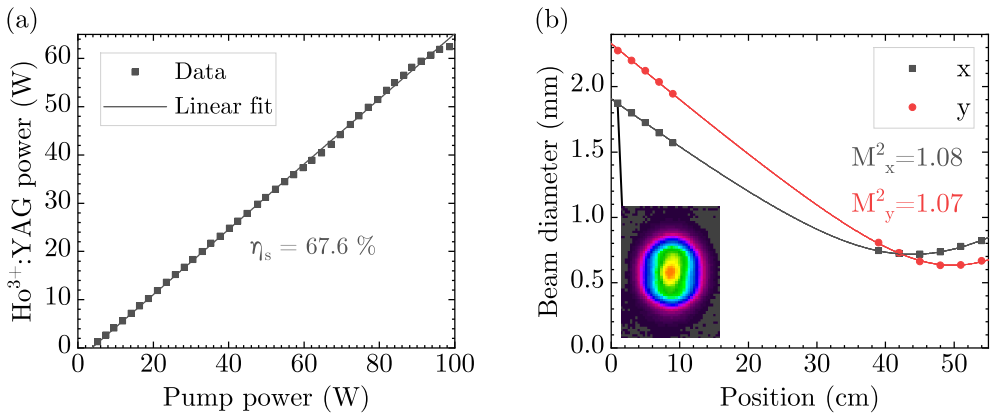

Fig. 2. (a) Output power of the Ho^{3+}:YAG pump source depending on the pump power. (b) Beam quality at a pump power of 89 W yielding an average output power of 58 W.

OPTICS CONTINUUM

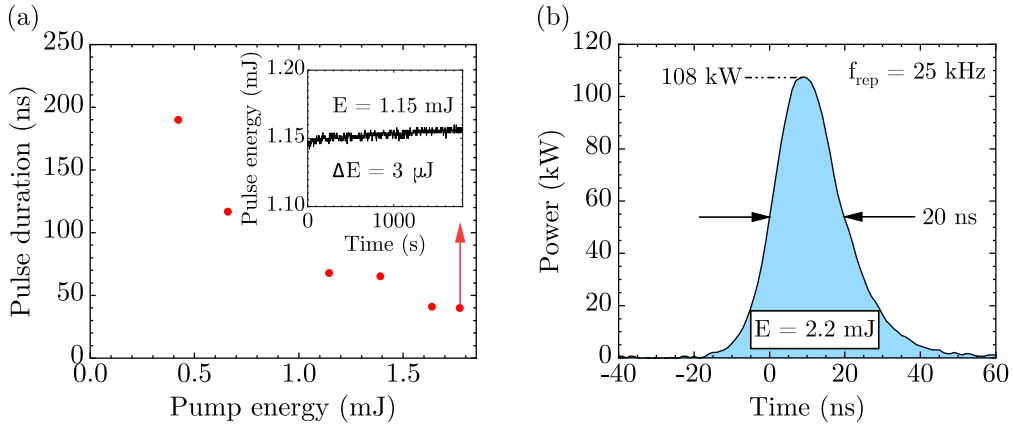

Fig. 3. (a) Pulse duration depending on the pump energy. The minimum pulse duration is 40 ns. The inset shows the pulse energy over a time of 30 min. (b) Exemplary temporal pulse shape at repetition rate of 25 kHz. A pulse peak power of 108 kW is reached.

especially pronounced when the laser is operated close to its stability limit which is the case at the chosen working point [25].

Figure 3(a) shows the pulse duration depending on the pump energy. At the working point, the pulse duration is 40 ns and the pulse energy of the laser output is stable over a time of 30 min with a standard deviation of 3 μJ (see inset of Fig. 3(a)). This results in a pulse peak power of 29 kW. For the application of pumping ZGP OPOs that have a pump threshold around 1 kW, high pulse peak powers are required. Therefore, the repetition rate of the laser is decreased to a minimum repetition rate of 25 kHz in order to remain below the damage threshold of the intracavity components. At this repetition rate, a pulse energy of 2.2 mJ and a pulse duration of 20 ns is measured which corresponds to a pulse peak power of 108 kW (see Fig. 3(b)).

Based on the data presented above, this laser source is well suited for pumping a ZGP OPO. It has an excellent beam quality which enables nearly planar phase fronts over the whole length of the nonlinear crystal. Furthermore, since the pulse peak power clearly surpasses the OPO threshold, an efficient conversion of the infrared laser pulses into the mid-IR range is enabled. The experimental setup of the OPO cavity is described in the next section.

4. Experimental setup of ZGP OPO

The schematic experimental setup of the ZGP OPO system is shown in Fig. 4. Besides the linear OPO resonator, it consists of beam shaping optics, the isolator needed to protect the laser resonator from reflections of components from the OPO, and two attenuators to control the pump power incident on the OPO as well as to limit the laser power to the rated value of the optical isolators. The power of the Ho^{3+}:YAG pump source is decreased to 40 W with a first attenuator consisting of a half-wave plate and a thin-film polarizer (TFP) in order to remain below the damage thresholds of the subsequent optical isolator which consists of a commercially available Faraday rotator and a TFP. The isolator is followed by another attenuator to control the input pump power coupled into the OPO and a half-wave plate to adjust the polarization to the ordinary crystal axis in order to meet the type I phase matching condition for an efficient conversion. A Galilean telescope is used to focus the pump beam to a $1/e^2$ beam diameter of 0.76 mm in order to not exceed any damage thresholds of the OPO cavity components. The doubly-resonant OPO cavity is formed by a plano-concave input coupling (IC) mirror with a radius of curvature of 0.1 m and a planar output coupling (OC) mirror. The IC mirror is highly transmissive for the pump

OPTICS CONTINUUM

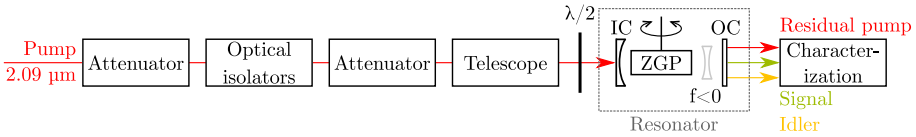

Fig. 4. Schematic representation of the linear ZGP OPO setup. The Ho^{3+}:YAG pump beam is attenuated and shaped to an appropriate pump diameter by a Galilean telescope. Furthermore, two optical isolators are inserted to protect the laser resonator from back reflections. A diverging lens can be inserted into the resonator to test different configurations.

wavelength (R<0.2% at 2.09 µm) and highly reflective for the mid-IR wavelengths (R>98% at 2.5 – 5µm). The OC mirror is highly transmissive for the pump wavelength (R<1% at 2.09 µm) and has a reflectivity of R = 50% at 3 – 5µm. The commercially available ZGP crystal (anti-reflection coated for 2 – 2.2µm and 3.5 – 4.8µm) has a size of 6mm × 6mm × 20mm and is cut to 55.5 °. The damage threshold of ZGP crystals is typically around 1 – 2 J cm^{-2} [28,29]. Consequently, a maximum fluence of 1 J cm^{-2} has not been exceeded. It is mounted in a copper mount and water-cooled to a temperature of 20 °. The crystal can be rotated about its vertical axis using a rotation stage to optimize the phase matching condition and maximize the output power. In the positive uniaxial crystal ZGP belonging to the $\bar{4}$2m crystal class [30], the type I phase-matching condition for the relevant difference-frequency generation mechanism is given by

$$\frac{n_o(\lambda_p)}{\lambda_p} = \frac{n_e(\theta, \lambda_s)}{\lambda_s} + \frac{n_e(\theta, \lambda_i)}{\lambda_i},$$

where λ_p is the pump wavelength, λ_s is the signal wavelength, and λ_i is the idler wavelength. n_o and n_e are the ordinary and extraordinary refractive indices and θ is the phase-matching angle. The effective nonlinearity of the ZGP crystal is given by

$$d_{\text{eff}} = d_{36} \cdot \sin(2\theta)$$

resulting in d_{eff} = 70.8 pm/V.

The total length of the OPO resonator was varied between 22 mm and 33 mm. As indicated above, the impact of an intracavity concave lens on the ZGP OPO is investigated by placing an anti-reflection coated CaF_2 lens in the longer OPO cavity. By varying the focal length of the concave lens (f = −0.1m, −0.08m, −0.05m), the mode size of the mid-IR radiation can precisely be adjusted to that of the pump mode. A characterization of these OPO cavities without and with different diverging lenses is presented in the following section.

5. Characterization of ZGP OPO

The characterization of the ZGP OPO is started with an assessment of the optical power characteristics. The total OPO output power (signal and idler power added up) depending on the pump power is shown in Fig. 5 for different resonator configurations. The slope efficiencies and pump thresholds for the 22 mm long cavity (black), the 33 mm long cavity without diverging lens (red), and the 33 mm long cavities with f = −0.1m (blue) and f = −0.08m (green) are similar. The highest slope efficiency of 52.1 % is reached in the configuration with f = −0.08m. The lowest pump threshold of 3.2 W is reached without any additional lens in the short cavity. All resonators except the 33 mm long one with the f = −0.05m lens reach similar output powers around 14 W. The low pump threshold in the short cavity is attributed to both the shortest round-trip time and the smallest resonator mode size in this case. When increasing the cavity length from 22 mm to 33 mm, the rise time of the OPO increases due to the decreased number of round trips in the cavity. This increases the threshold power and is consistent with the black and

OPTICS CONTINUUM

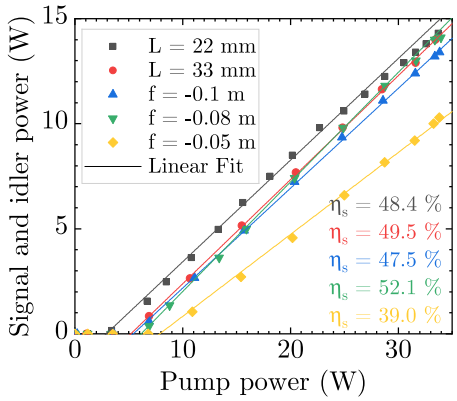

Fig. 5. Total mid-IR output power depending on the pump power. Power-power curves are shown for the OPOs without additional lens (22 mm (black) and 33 mm long (red)), and for the 33 mm long cavities with $f = -0.1$m (blue), $f = -0.08$m (green), and $f = -0.05$m (yellow). The measurement error is below 3%.

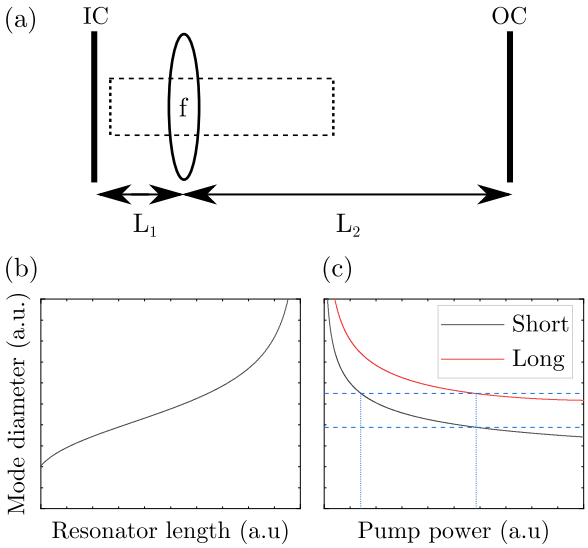

Fig. 6. (a) Plane-plane OPO cavity including a thermal lens with focal length f. (b) Cavity mode size depending on the resonator length assuming a fixed thermal lens. (c) Cavity mode size depending on the pump power for a short and a long resonator in comparison. At a fixed pump power, the cavity mode is larger in the longer cavity. Conversely, the same mode size is reached at a higher pump power in the long cavity.

red curve shown in Fig. 5. In the longer cavities including the diverging lenses, the increase in threshold power can be attributed to the increased mode sizes in the cavity. Illustratively, this can be explained with the stability criteria for a resonator which contains a thermal lens presented in [31].

In a simple plane-plane resonator with a thermal lens with focal length f and distances L_1 and L_2 of the thermal lens from the mirrors, the mode size at the position of the thermal lens (effectively in the ZGP crystal) increases with increasing resonator length. A scheme of the corresponding situations and the expected modeled dependence is shown in Fig. 6(a) and (b),

OPTICS CONTINUUM

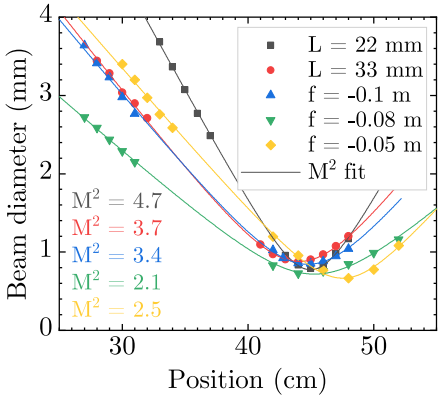

Fig. 7. Beam quality measurements of signal beams for different cavity configurations (22 mm long cavity (black) and 33 mm long cavity without additional lens (red), with $f = -0.1$m lens (blue), with $f = -0.08$m lens (green), and with $f = -0.05$m lens (yellow)).

respectively. For a fixed resonator length and a thermal focal length which is considerably larger than the resonator length, the mode size is expected to decrease with increasing refractive power of the thermal lens. Consequently, in two resonators with different lengths the same mode sizes are reached for a stronger thermal lens in the longer resonator (see Fig. 6(c)). Since the refractive power of the thermal lens increases with increasing pump power, this explains the higher pump threshold in the longer resonator. In analogy to this, an additional diverging lens in the cavity has the opposite effect of the (in ZGP: positive) thermal lens and effectively increases the mode size at the position of the thermal lens and consequently, the threshold shifts to higher pump powers. This can explain why the resonator configuration using the diverging lens with $f = -0.05$m leads to a considerably lower slope efficiency and maximum output power.

The specific cavity configuration does not only influence the threshold pump power and the maximum output power, but it has a strong influence on the beam quality as well. Fig. 7 shows exemplarily beam quality measurements for the signal beam for the different cavity configurations at a pump power of 34 W. The beam quality of the idler beam behaves in analogy to the signal beam but the beam quality factor tends to be slightly higher. For reasons of clarity, the beam quality is only shown for the vertical beam axis. Two observations can be made. Firstly, the beam quality improves in the longer cavity since the intrinsic mode size of the cavity increases in the longer resonator and therefore, better fits to the pump diameter. Secondly, with the same reasoning, the beam quality improves when using the lenses with $f = -0.1$m and $f = -0.08$m. For $f = -0.05$m, a deterioration in beam quality is observed which might result from a signal and idler mode larger than the pump mode. This is probably also the reason for the observed strong decrease in output power and slope efficiency when the $f = -0.05$m lens is used. Taking both the power and the beam quality measurements together, the optimum resonator configuration for the given pump spot diameter is the 33 mm long cavity with the $f = -0.08$m lens which is characterized in more detail in the following paragraph.

The maximum output power in this configuration is 14.1 W at a pump power of 34 W (see Fig. 8). Taking into account the residual pump power of 5.7 W, a conversion efficiency of 49.8 % results. Figure 8 also shows the beam quality of the signal beam depending on the pump power which has been determined by separating the signal and idler beam with a dichroic filter. The beam quality deteriorates with increasing pump power since the refractive power of the thermal lens increases which in turn decreases the mode size of the signal mode. An increasing M^2 value means that the mismatch between signal and pump mode increases. The different beam quality factors in the two beam axes result from the astigmatic nature of the pump beam. Fig. 9(a) and

OPTICS CONTINUUM

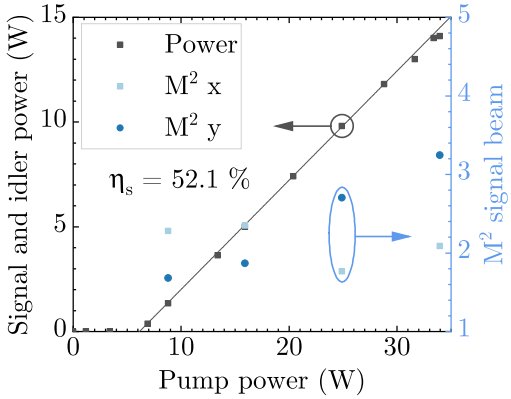

Fig. 8. Total OPO power and beam quality of the signal beam depending on the pump power (resonator with $f = -0.08$m lens). With increasing pump power, the beam quality deteriorates due to an increasing mode mismatch of pump and signal mode.

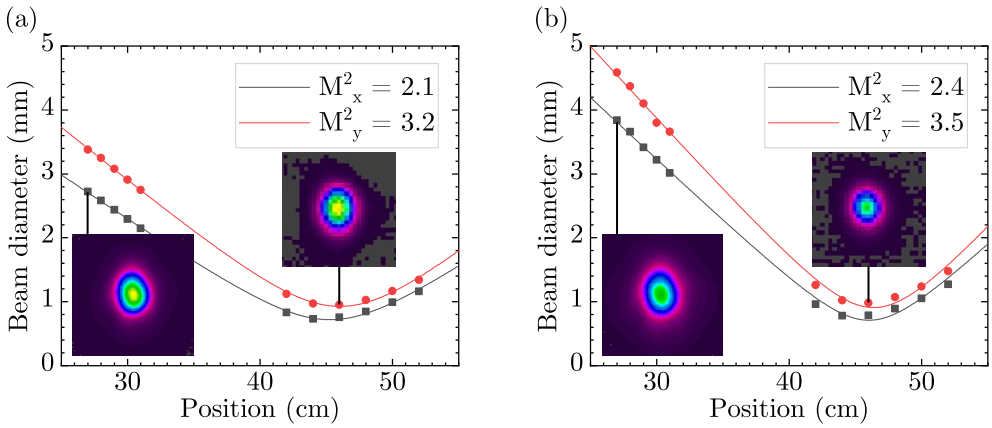

Fig. 9. Beam quality of the signal (a) and idler (b) beam at 14.1 W OPO output power (resonator with $f = -0.08$m lens).

(b) show beam quality measurements of the signal and idler beam, respectively, at a pump power of 34 W. The M^2 value of the signal beam is 2.1 in the x-axis and 3.2 in the y-axis of the beam and the M^2 value of the idler beam is 2.4 in the x-axis and 3.6 in the y-axis of the beam. In contrast to this, in the 22 mm long resonator, the M^2 value of the signal beam was measured to be 4.7 in the x-axis and 6.6 in the y-axis and the M^2 value of the idler beam was measured to be 4.5 in the x-axis and 6.3 in the y-axis. Although better beam quality results have been obtained by other research groups, e.g. M^2<1.5 at 4.2 W OPO output power by Budni et al. [18] and $M^2 \approx 2.7$ at 12.6 W OPO output power by Elder [21], it should be clarified that the aim of this work is to show that a beam quality improvement is possible by inserting an intracavity lens.

Figure 10 shows an exemplary pulse from the pump source and the OPO output. The OPO pulse has an energy of 0.56 mJ and a pulse duration of 17 ns which is slightly lower than the pump pulse duration. This results from the high OPO threshold power which is required for the nonlinear conversion. Consequently, at the rising and falling edge of the pulse, the pump light is not converted since the power is below the OPO threshold which results in the shorter OPO pulse duration. While the pulse energy stability of the pump pulse was measured to be 1.3 %, the pulse energy stability of the OPO output pulse was measured to be 2.3 %. The pulse energy stability

OPTICS CONTINUUM

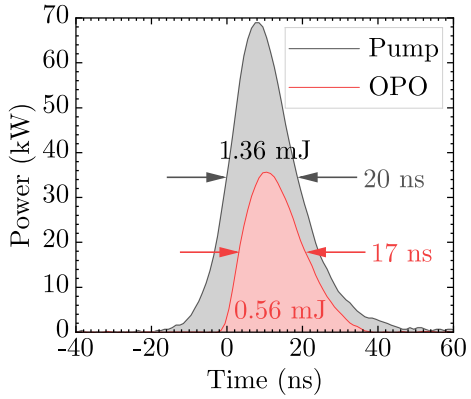

Fig. 10. Comparison of pump pulse and OPO output pulse at a pump power of 34 W corresponding to an output power of 14 W (resonator with $f = -0.08$m lens).

was determined by measuring the pulse energy of a set of 125 pulses and calculating the root mean square deviation.

6. Conclusion

We presented an efficient and compact Ho^{3+}:YAG pump source emitting 2.09 µm radiation with a pulse energy of 2.2 mJ and a pulse duration of 20 ns when operated at 25 kHz repetition rate, well suited for pumping ZGP OPOs. The beam quality is below M^2<1.1. This source was used to pump a linear doubly-resonant ZGP OPO. Investigations for improving the beam quality in this low-complexity resonator type were presented. Both a longer resonator as well as a diverging intracavity lens increase the signal and idler fundamental mode size in the OPO cavity. Consequently, the mismatch between pump and signal mode at higher pump powers decreases which results in an improvement of beam quality at higher output powers. In the optimum configuration with a 33 mm long resonator including a $f = -0.08$m intracavity lens, a total OPO output power of 14.1 W is measured at a pump power of 34 W. OPO pulses with an energy of 0.56 mJ and a pulse duration of 17 ns are generated with this linear OPO. The beam quality at maximum output power is 2.1 and 3.2 in the x- and y-axis of the signal beam and 2.4 and 3.6 in the x- and y-axis of the idler beam. This is not only a clear improvement to the 22 mm long cavity without intracavity lens that showed beam quality factors of 4.7 and 6.6 in the x- and y-axis of the signal and 4.5 and 6.3 in the x- and y-axis of the idler beam but also an improvement compared to the 33 mm long cavity that showed beam quality factors of 3.7 and 5.6 in the x- and y-axis of the signal and 4.4 and 6.0 in the x- and y-axis of the idler beam. The presented results show the importance and influence of mode matching between the pump and mid-IR modes and pave the way for further scaling of the OPO output power while maintaining a high beam quality.

Funding. Bundesministerium der Verteidigung.

Acknowledgments. We acknowledge the support of the mechanical workshop of the Fraunhofer IOSB and Artur Schander who fabricated special opto-mechanical components for the experimental setup.

Disclosures. The authors declare no conflicts of interest.

Data availability. Data underlying the results presented in this paper are not publicly available at this time but may be obtained from the authors upon reasonable request.

References

1. V. S. Serebryakov, E. V. Boiko, A. G. Kalintsev, *et al.*, "Mid-IR laser for high-precision surgery," J. Opt. Technol. **82**(12), 781–788 (2015).

OPTICS CONTINUUM

2. S. Naithani, A. Grisard, D. Schaubroeck, *et al.*, "Mid-infrared resonant ablation of PMMA," J. Laser Micro/Nanoeng. **9**(2), 147–152 (2014).
3. A. Sijan, "Development of military lasers for optical countermeasures in the mid-IR," in *Technologies for Optical Countermeasures VI*, vol. 7483 (SPIE, 2009), pp. 32–45.
4. Q. Lu, S. Slivken, D. Wu, *et al.*, "High power continuous wave operation of single mode quantum cascade lasers up to 5 W spanning $\lambda \sim 3.8 - 8.3$ µm," Opt. Express **28**(10), 15181–15188 (2020).
5. F. Maes, V. Fortin, M. Bernier, *et al.*, "5.6 W monolithic fiber laser at 3.55 µm," Opt. Lett. **42**(11), 2054–2057 (2017).
6. F. Maes, V. Fortin, S. Poulain, *et al.*, "Room-temperature fiber laser at 3.92 µm," Optica **5**(7), 761–764 (2018).
7. J. Kernal, V. V. Fedorov, A. Gallian, *et al.*, "3.9–4.8 µm gain-switched lasing of Fe:ZnSe at room temperature," Opt. Express **13**(26), 10608–10615 (2005).
8. M. E. Doroshenko, H. Jelínková, T. T. Basiev, *et al.*, "Fe:ZnSe laser - comparison of active materials grown by two different methods," in *Solid State Lasers XX: Technology and Devices*, vol. 7912 W. A. Clarkson, N. Hodgson, and R. Shori, eds., International Society for Optics and Photonics (SPIE, 2011), p. 79122D.
9. M. R. Majewski, R. I. Woodward, and S. D. Jackson, "Dysprosium mid-infrared lasers: current status and future prospects," Laser Photonics Rev. **14**(3), 1900195 (2020).
10. G. Liu, S. Mi, K. Yang, *et al.*, "161 W middle infrared $ZnGeP_2$ MOPA system pumped by 300 W-class Ho:YAG MOPA system," Opt. Lett. **46**(1), 82–85 (2021).
11. M. Eichhorn, M. Schellhorn, M. W. Haakestad, *et al.*, "120-mJ mid-infrared $ZnGeP_2$ FIRE OPO," in *Nonlinear Optics*, (Optical Society of America, 2015), pp. NTu1B–5.
12. K. L. Vodopyanov, "Parametric generation of tunable infrared radiation in $ZnGeP_2$ and GaSe pumped at 3 µm," J. Opt. Soc. Am. B **10**(9), 1723–1729 (1993).
13. G. D. Boyd, E. Buehler, and F. G. Storz, "Linear and nonlinear optical properties of $ZnGeP_2$ and CdSe," Appl. Phys. Lett. **18**(7), 301–304 (1971).
14. J. D. Beasley, "Thermal conductivities of some novel nonlinear optical materials," Appl. Opt. **33**(6), 1000–1003 (1994).
15. M. Eichhorn, "Quasi-three-level solid-state lasers in the near and mid infrared based on trivalent rare earth ions," Appl. Phys. B **93**(2-3), 269–316 (2008).
16. M. Griesbeck, H. Büker, M. Eitner, *et al.*, "Mid-infrared optical parametric oscillator pumped by a high-pulse-energy, Q-switched Ho^{3+}:YAG laser," Appl. Opt. **60**(22), F21–F26 (2021).
17. K. Goth, M. Griesbeck, M. Eitner, *et al.*, "Alignment-insensitive end-pumped continuous-wave crossed-Porro prism Ho^{3+}:YAG laser," Opt. Lett. **47**(13), 3143–3146 (2022).
18. P. A. Budni, L. A. Pomeranz, M. L. Lemons, *et al.*, "Efficient mid-infrared laser using 1.9-µm-pumped Ho:YAG and $ZnGeP_2$ optical parametric oscillators," J. Opt. Soc. Am. B **17**(5), 723–728 (2000).
19. E. Lippert, S. Nicolas, G. Arisholm, *et al.*, "Midinfrared laser source with high power and beam quality," Appl. Opt. **45**(16), 3839–3845 (2006).
20. S. Bigotta, G. Stöppler, J. Schöner, *et al.*, "Novel non-planar ring cavity for enhanced beam quality in high-pulse-energy optical parametric oscillators," Opt. Mater. Express **4**(3), 411–423 (2014).
21. I. Elder, "Thulium fibre laser pumped mid-IR source," in *Laser Technology for Defense and Security V*, vol. 7325 (SPIE, 2009), pp. 98–108.
22. A. Hemming, J. Richards, A. Davidson, *et al.*, "99 W mid-IR operation of a ZGP OPO at 25% duty cycle," Opt. Express **21**(8), 10062–10069 (2013).
23. G. Arisholm, R. Paschotta, and T. Südmeyer, "Limits to the power scalability of high-gain optical parametric amplifiers," J. Opt. Soc. Am. B **21**(3), 578–590 (2004).
24. C.-P. Qian, B.-Q. Yao, B.-R. Zhao, *et al.*, "High repetition rate 102 W middle infrared $ZnGeP_2$ master oscillator power amplifier system with thermal lens compensation," Opt. Lett. **44**(3), 715–718 (2019).
25. K. Goth, M. Rupp, M. Griesbeck, *et al.*, "Limitations of homogeneous and segmented single-crystal compact TEM_{00}-mode Ho^{3+}:YAG laser resonators," Appl. Phys. B **129**(6), 95 (2023).
26. W. Koechner, "Thermal lensing in a Nd:YAG laser rod," Appl. Opt. **9**(11), 2548–2553 (1970).
27. D. Hanna, "Astigmatic Gaussian beams produced by axially asymmetric laser cavities," IEEE J. Quantum Electron. **5**(10), 483–488 (1969).
28. M. W. Haakestad, H. Fonnum, and E. Lippert, "Mid-infrared source with 0.2 J pulse energy based on nonlinear conversion of Q-switched pulses in $ZnGeP_2$," Opt. Express **22**(7), 8556–8564 (2014).
29. A. Hildenbrand, C. Kieleck, A. Tyazhev, *et al.*, "Laser damage of the nonlinear crystals $CdSiP_2$ and $ZnGeP_2$ studied with nanosecond pulses at 1064 and 2090 nm," Opt. Eng. **53**(12), 122511 (2014).
30. P. E. Powers, *Field Guide to Nonlinear Optics* (SPIE, 2013).
31. V. Magni, "Multielement stable resonators containing a variable lens," J. Opt. Soc. Am. A **4**(10), 1962–1969 (1987).